Mayer, R. P., and R. A. Stowe, "Mercury Porosimetry: Filling of Toroidal Void Volume Following Breakthrough between Packed Spheres," *J. Phys. Chem.*, **70**, 3867 (1966).
Nenninger, E., Jr., and J. A. Storrow, "Drainage of Packed Beds in Gravitational and Centrifugal-Force Fields," *AIChE J*, **4**, 305 (1958).
Princen, H. M., "Capillary Pheonomena in Assemblies of Parallel Cylinders. I. Capillary Rise between Two Cylinders," *J. Colloid Interface Sci.*, **30**, 69 (1969a).
———, "Capillary Phenomena in Assemblies of Parallel Cylinders. II. Capillary Rise between Systems with More than Two Cylinders," *ibid.*, 359 (1969b).
Ritter, H. L., and L. C. Drake, "Pore-Size Distribution in Porous Media: Pressure Porosimeter and Determination of Complete Macropore-Size Distributions," *Ind. Eng. Chem. Anal. Ed.*, **17**, 782 (1945).
Storrow, J. A., "Hydroextraction: Flow in Submerged Cakes," *AIChE J.*, **3**, 528 (1957).

Manuscript received August 10, 1971; revision received May 3, 1973, and accepted May 4, 1973.

Combined Forced and Free Convection Flow Past a Horizontal Flat Plate

The problem of simultaneous forced and free convection flow of a Newtonian fluid past a hot or cold horizontal flat plate is investigated by means of numerical solutions of the full equations of motion and thermal energy subject only to the Boussinesq approximation. These solutions span the parameter ranges $10 \leq Re \leq 100$, $0.1 \leq Pr \leq 10$, and $-2.215 \leq Gr/Re^{5/2} \leq 2.215$ where Re, Pr, and Gr are based on the ambient free stream fluid properties and the overall plate length l. When $Gr > 0$, the boundary flow near the plate surface is accelerated relative to the corresponding forced convection flow, with a resulting increase in both the local skin friction and heat transfer coefficients. When $Gr < 0$, the boundary flow is decelerated, the local skin friction and heat transfer are decreased, and the flow actually separates for $Gr/Re^{5/2} < -0.8$ when $Pr = 0.7$. In the latter circumstance, an increasing degree of upstream influence is observed as $Gr/Re^{5/2}$ is further decreased.

G. E. ROBERTSON
J. H. SEINFELD
and L. G. LEAL

Department of Chemical Engineering
California Institute of Technology
Pasadena, California 91109

SCOPE

The buoyancy effects induced by a hot or cold body can cause considerable deviations from the basic forced convection flow which would exist when the body and free stream fluid are at the same temperature. In some circumstances, such deviations may be of significance primarily because of the accompanying changes in the overall heat transfer rate; however, in general, one would be interested in a detailed understanding of the changes in flow structure, and a considerable body of literature has grown up in an attempt to achieve this goal. To date, the majority of this work has been concerned with the case in which a significant component of the buoyancy-induced body force is either parallel or antiparallel with the direction of the undisturbed fluid motion [compare the work of Acrivos (1966), Merkin (1969), and others on the combined forced and free convection flow past a vertical flat plate].

In this work, we utilize numerical solutions of the full equations of motion and thermal energy, subject to the Boussinesq approximation, to consider the laminar, two-dimensional flow of a Newtonian fluid past the upper surface of a hot or cold horizontal flat plate. The most significant previous investigations of this problem are the boundary-layer analyses of Sparrow and Minkowycz (1962) and Leal (1973a). In these papers, it is shown that the cross-stream buoyancy-induced body force acts effectively to produce a streamwise pressure gradient in the fluid adjacent to the plate surface: favorable, in the usual

Correspondence concerning this paper should be addressed to L. G. Leal.

boundary-layer sense, when the plate is hot, and adverse when the plate is cold. Hence, the local boundary flow is either accelerated or decelerated relative to the corresponding forced convection flow, and the local skin friction and heat transfer are predicted either to increase or decrease depending upon whether the plate is hot or cold. Although these results are of considerable interest, the corresponding analyses are strictly limited to situations in which the natural convection contribution remains as a small correction to the basic forced convection flow. In particular, although the basic boundary flow is decelerated near the plate surface and hence has the potential to separate, an explicit prediction of this effect is outside the scope of the existing boundary-layer analyses.

The present paper is thus addressed to two main points. First, what is the qualitative nature of the flow produced when the effect of buoyancy is not small; and, second, what is the particular nature of the fluid motion when the plate is sufficiently cold so that the boundary flow actually separates? Additionally, we consider the role of the fluid Prandtl number in determining the flow structure under these circumstances. In this paper, we concentrate particularly on the region in the immediate vicinity of the plate.

CONCLUSIONS AND SIGNIFICANCE

Numerical solutions of the full equations of motion and thermal energy have been obtained subject to the Boussinesq approximation for $10 \leq Re \leq 100$, $0.1 \leq Pr \leq 10$, and $-2.215 \leq Gr/Re^{5/2} \leq 2.215$, where Re is the Reynolds number, Pr the Prandtl number, and Gr the Grashof number based on the ambient, free stream fluid properties and the overall plate length l.

For the intermediate values of Re investigated, the flow structure erhibits the same qualitative features as predicted by existing boundary-layer theories which are valid for $Re \rightarrow \infty$ and $|Gr/Re^{5/2}| << 1$. Thus, the gravitationally induced streamwise pressure gradient produces either an acceleration or deceleration of the boundary flow compared with the corresponding forced convection case ($Gr = 0$) depending on whether the plate surface is hot or cold. When $Gr > 0$ and is increased, the local skin friction and heat transfer coefficients increase over the plate surface, and the flow structure remains qualitatively the same even as $|Gr/Re^{5/2}| = 0(1)$. On the other hand, when $Gr/Re^{5/2} < -0.8$ (for $Pr = 0.7$), the buoyancy-induced streamwise pressure gradient actually causes the flow to separate and a recirculating eddy develops adjacent to the plate surface. As Gr is further decreased, the recirculating eddy increases in size; but, more importantly, its leading edge moves forward along the plate surface until, finally, the reverse flow region is found to extend upstream beyond the leading edge of the plate. As Re or Pr is decreased, with $Gr/Re^{5/2}$ fixed, the size of the recirculating eddy is increased, as is the extent of its upstream influence on the flow. Finally, it should be noted that the onset of separation and growth of a large recirculating eddy is accompanied by a rather remarkable decrease in the overall frictional drag on the plate, as well as a smaller decrease in the overall heat transfer coefficient.

The presence of a recirculating flow upstream beyond the leading edge of the plate is, perhaps, the most interesting and significant result of the present work. Careful observation of the temperature, vorticity, and stream-function fields in a time-dependent numerical solution indicates that the mechanism for the progressive (in time) upstream movement of the recirculating eddy lies in the local stable density stratification which is produced as the fluid adjacent to the plate surface is cooled below the ambient, free stream temperature. It is, of course, well known that the presence of a finite two-dimensional body (in this case the recirculating eddy) can produce strong upstream disturbances when the ambient fluid is stably stratified; however, so far as we are aware, the presence of significant upstream influence due to a locally induced stratification has not hitherto been reported in the literature.

PHYSICAL PROBLEM AND BASIC EQUATIONS

We consider the laminar, two-dimensional motion of Newtonian fluid past a hot or cold flat plate of length l. As indicated in Figure 1, the free stream velocity and temperature are denoted by U_∞ and T_∞, the temperature at the upper surface of the plate by $T_\infty + \Delta T$, and the streamwise and normal coordinate directions by x and y. We are primarily concerned in this work with understanding the role of the temperature induced buoyancy forces in contributing to the flow structure in the immediate vicinity of the plate surface. Hence, in order to simplify the analysis, we consider the case in which the plate, as a whole, acts as a heat dipole; that is, we consider the temperature of the underside of the plate to be $T_\infty - \Delta T$, corresponding to a situation in which there is no net heat transfer to the ambient fluid. The advantage of this choice is that the velocity field produced is thereby symmetric about the plane $y = 0$. The alternate source problem, in which the underside temperature is $T_\infty + \Delta T$ is also of interest; however, it can be anticipated from boundary-layer theory that the detailed structure of the velocity and temperature fields in the immediate vicinity of either the upper or lower surface of the plate will be essentially the same for the source and dipole problems in spite of the

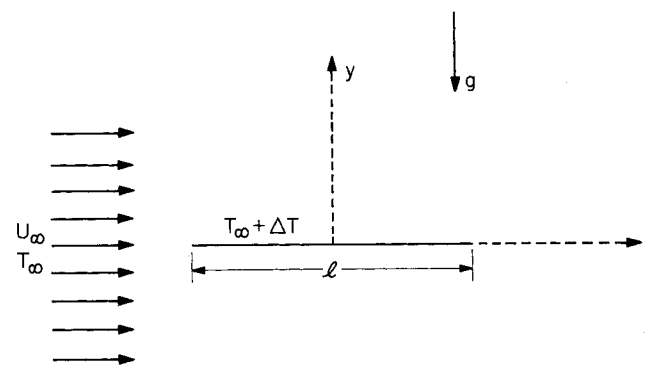

Fig. 1. The physical system.

fact that the structure of the downstream wake regions will be markedly different (a point which we shall consider in detail in a later communication).

Nondimensionalizing the basic conservation balances for momentum, mass, and thermal energy using the ambient (free stream) fluid properties, the free-stream velocity U_∞ and the plate length l, and invoking the usual Boussinesq approximation (Boussinesq, 1903; Spiegel and Veronis, 1960), we obtain the basic governing differential equations

$$\frac{\partial u}{\partial t} + u\frac{\partial u}{\partial x} + v\frac{\partial u}{\partial y} = -\frac{\partial p}{\partial x} + \frac{1}{Re}\left(\frac{\partial^2 u}{\partial x^2} + \frac{\partial^2 u}{\partial y^2}\right) \tag{1a}$$

$$\frac{\partial v}{\partial t} + u\frac{\partial v}{\partial x} + v\frac{\partial v}{\partial y} = -\frac{\partial p}{\partial y} + \frac{1}{Re}\left(\frac{\partial^2 v}{\partial x^2} + \frac{\partial^2 v}{\partial y^2}\right) + \frac{Gr}{Re^2}\theta \tag{1b}$$

$$\frac{\partial u}{\partial x} + \frac{\partial v}{\partial y} = 0 \tag{2}$$

$$\frac{\partial \theta}{\partial t} + u\frac{\partial \theta}{\partial x} + v\frac{\partial \theta}{\partial y} = \frac{1}{PrRe}\left(\frac{\partial^2 \theta}{\partial x^2} + \frac{\partial^2 \theta}{\partial y^2}\right) \tag{3}$$

in which

$$Re = \frac{\rho_\infty U_\infty l}{\mu_\infty}, \quad Pr = \frac{C_{p\infty}\mu_\infty}{k_\infty}, \quad \text{and} \quad Gr = \frac{l^3\beta g \Delta T \rho_\infty^2}{\mu_\infty^2}$$

where θ is defined as $(T - T_\infty)/\Delta T$, β is the coefficient of thermal expansion, and the subscript ∞ represents the free stream value.

With the present definition, it may be noted that $Gr > 0$ corresponds to the case in which the upper plate surface is hot relative to the ambient fluid, whereas $Gr < 0$ corresponds to the case in which it is cold. Clearly, the relevant buoyancy parameter is Gr/Re^2 according to (1). Leal (1973a) and Sparrow and Minkowycz (1962) both show that the equivalent parameter in the boundary-layer version of (1) to (3) is $Gr/Re^{5/2}$, a result which we shall utilize at a later point.

In view of the symmetry of the dipole problem, these equations need only be solved in the upper half plane. The appropriate boundary conditions are simply

$$\frac{\partial u}{\partial y} = v = \theta = 0 \quad ; \quad |x| > \frac{1}{2}, \; y = 0 \tag{4a}$$

$$u = v = 0, \; \theta = 1 \quad ; \quad |x| \leq \frac{1}{2}, \; y = 0 \tag{4b}$$

$$u \to 1, \; v \to 0, \; \theta \to 0; \quad r = (x^2 + y^2)^{1/2} \to \infty \tag{4c}$$

For purposes of obtaining a numerical solution to this problem, it is convenient to rewrite Equations (1) to (4) in terms of the streamfunction ψ and vorticity ω, defined by

$$u = \frac{\partial \psi}{\partial y}, \quad v = -\frac{\partial \psi}{\partial x}, \quad \omega = \frac{\partial v}{\partial x} - \frac{\partial u}{\partial y}$$

and to transform the resulting equations to an elliptical cylindrical coordinate system (ξ, η) in which

$$x = \frac{1}{2}\cosh\xi\cos\eta, \quad y = \frac{1}{2}\sinh\xi\sin\eta \tag{5}$$

hence yielding the governing equations

$$\frac{1}{4}M^2(\xi,\eta)\frac{\partial \omega}{\partial t} + J(\omega,\psi) = \frac{1}{Re}\left(\frac{\partial^2 \omega}{\partial \xi^2} + \frac{\partial^2 \omega}{\partial \eta^2}\right) + \frac{Gr}{2Re^2}\left(\sinh\xi\cos\eta\frac{\partial \theta}{\partial \xi} - \cosh\xi\sin\eta\frac{\partial \theta}{\partial \eta}\right) \tag{6}$$

$$\frac{\partial^2 \psi}{\partial \xi^2} + \frac{\partial^2 \psi}{\partial \eta^2} + \frac{1}{4}M^2(\xi,\eta)\,\omega = 0 \tag{7}$$

$$\frac{1}{4}M^2(\xi,\eta)\frac{\partial \theta}{\partial t} + J(\theta,\psi) = \frac{1}{PrRe}\left(\frac{\partial^2 \theta}{\partial \xi^2} + \frac{\partial^2 \theta}{\partial \eta^2}\right) \tag{8}$$

where $M^2(\xi,\eta) = \frac{1}{2}(\cosh 2\xi - \cos 2\eta)$ and the nonlinear, two-dimensional Jacobian is given by

$$J(\alpha,\gamma) = \frac{\partial \alpha}{\partial \xi}\frac{\partial \gamma}{\partial \eta} - \frac{\partial \alpha}{\partial \eta}\frac{\partial \gamma}{\partial \xi}$$

The advantage of elliptical cylindrical coordinates is that the region near the plate is effectively magnified, particularly the singular regions near the ends of the plate which are effectively resolved by a corresponding coordinate singularity (Leal and Acrivos, 1969). In this coordinate system the plate is located at $\xi = 0$, and the remaining portions of the x-axis ($|x| > \frac{1}{2}$, $y = 0$) are given by $\eta = 0$ ($x > \frac{1}{2}$) and $\eta = \pi$ ($x < -\frac{1}{2}$), respectively. Hence, the boundary conditions (4) can be expressed as

$$\psi = \omega = \theta = 0; \quad \eta = 0 \text{ and } \pi, \quad \text{all } \xi > 0 \tag{9a}$$

$$\frac{\partial \psi}{\partial \xi} = \psi = 0; \quad \theta = 1; \quad \xi = 0, \quad 0 \leq \eta \leq \pi \tag{9b}$$

and

$$\psi \to \frac{1}{2}\sinh\xi\sin\eta, \quad \omega \to 0, \quad \theta \to 0; \quad \xi \to \infty, \quad 0 \leq \eta \leq \pi \tag{9c}$$

We shall be concerned, in this paper, with the numerical solution of the problem represented by Equations (6) to (9).

NUMERICAL SOLUTION SCHEME

The basic numerical solution scheme utilized in this work was based on the explicit, Gauss-Seidel pointwise iteration applied to the appropriate finite-difference form of the Equations (6) to (9), with $\partial\theta/\partial t$ and $\partial\omega/\partial t$ set equal to zero. This steady state iterative algorithm (which is similar to that of Leal and Acrivos, 1969) converges more rapidly to the final steady state than most standard time-dependent schemes and hence was used to obtain all of the steady state solutions which comprise the major portion of the present investigation. The finite-difference approximations of (6) to (8) were obtained using the simple two-point central difference formula for spatial first derivatives and the familiar five-point approximation for the Laplacian operator. Hence they are accurate to $0(h^2)$, where h is the computational mesh size in the (ξ, η) plane. The more stable Arakawa (1966) eight-point approximation for the nonlinear Jacobians was also utilized in several cases with no discernable change in results. The influence of computational mesh size on the solution was carefully documented in every instance, and the final values used are listed in Table 1. Finally, it should be noted that two minor modifications of the straightforward iterative scheme were made to enhance numerical stability. First, relaxation parameters a_ψ, a_ω, and a_θ, chosen by numerical experimentation, were introduced such that the values of ψ, ω, and θ retained at each mesh point for use in subsequent calculations were a weighted average of the value from the previous iteration and the newly computed

TABLE 1. NUMERICAL PARAMETERS

Re	Gr/Re^2	Pr	h	x_∞	a_ψ	a_ω	a_θ
10	+7	0.7	$\pi/30$	5.8(11.6)	1.1	0.4	0.4
10	+5	0.7	$\pi/30$	5.8	1.1	0.4	0.4
10	0	0.7	$\pi/30$	5.8(11.6)	1.1	0.4	0.4
10	−5	0.7	$\pi/30$	11.6(17.4)	1.0	0.2	0.2
10	−7	0.7	$\pi/30$	11.6(17.4)	1.0	0.2	0.2
40	+8	10.0	$\pi/50$	3.08	0.7	0.05	0.05
40	+8	0.7	$\pi/50$	3.08	1.1	0.4	0.4
40	+5	0.7	$\pi/50$	3.08	1.1	0.4	0.4
40	0	10.0	$\pi/50$	3.08(1.54)	1.1	0.4	0.05
40	0	0.7	$\pi/50$	3.08(6.16)	1.1	0.4	0.4
40	−5	0.7	$\pi/50$	6.16(3.08)	1.0	0.2	0.2
40	−7	0.7	$\pi/50$	9.24(6.16)	0.9	0.1	0.1
40	−8	0.7	$\pi/50$	9.24(12.32)	0.9	0.1	0.1
40	−11	10.0	$\pi/50$	3.08	0.7	0.05	0.05
40	−11	0.7	$\pi/50$	9.24(12.32)	0.9	0.1	0.1
40	−14	0.7	$\pi/50$	9.24(12.32)	0.9	0.1	0.1
100	+14	0.7	$\pi/60$	2.5	1.1	0.4	0.4
100	0	10.0	$\pi/60$	2.5	1.1	0.4	0.025
100	0	0.7	$\pi/60$	2.5	1.1	0.4	0.4
100	0	0.1	$\pi/60$	7.5	1.1	0.4	1.5
100	−11	0.7	$\pi/60$	5.0(7.5)	1.0	0.2	0.2
100	−14	0.7	$\pi/60$	5.0(7.5)	1.0	0.2	0.2
100	−22.15	0.7	$\pi/60$	5.0(7.5)	0.7	0.025	0.025

value; for example,

$$\omega_{\text{retained}} = \omega_{\text{old}} + a_\omega(\omega_{\text{new}} - \omega_{\text{old}}) .$$

The values of a_ψ, a_θ, and a_ω utilized in each case are listed in Table 1. Secondly, the calculations were actually performed in terms of $\hat{\psi}$ rather than ψ, where $\hat{\psi} = \psi - \frac{1}{2}\sinh\xi\sin\eta$.

In applying the boundary conditions (9b), the no-slip condition at the plate surface, $\partial\psi/\partial\xi|_{\xi=0} = 0$ was replaced by an equivalent condition relating the surface vorticity ω_0 to the values of the streamfunction on adjacent rows (Leal and Acrivos, 1969). Utilizing a Taylor series expansion, the value of the streamfunction ψ_1 at $\xi = h$ can be expressed in terms of ψ and its derivatives at the plate surface as

$$\psi_1 = \psi|_{\xi=0} + h\left.\frac{\partial\psi}{\partial\xi}\right|_{\xi=0} + \frac{h^2}{2!}\left.\frac{\partial^2\psi}{\partial\xi^2}\right|_{\xi=0} + 0(h^3) \tag{10}$$

Utilizing Equation (7) and the boundary conditions (9b), and truncating series (10) after the term of $0(h^2)$, we obtain

$$\omega_0 = -\frac{8\psi_1}{h^2M^2(0,\eta)} + 0(h) \tag{11}$$

Similarly, by including the term of $0(h^3)$, a more accurate condition can be derived in terms of ψ_1 and ψ_2 $(\psi|_{\xi=2h})$,

$$\omega_0 = \frac{2(\psi_2 - 8\psi_1)}{h^2M^2(0,\eta)} + 0(h^2) \tag{12}$$

However, for the fluid motion problem alone [that is, Equations (6) and (7) with $Gr = 0$ and appropriate boundary conditions], the expression (12) is less stable than (11) in the numerical scheme (compare Thom and Apelt, 1956; Janssen, 1957; Leal and Acrivos, 1969). Therefore, relation (11) was employed for the majority of each calculation with the more accurate formula (12) being used only as a check on the solution once convergence was achieved.

The most troublesome feature of the present calculations, at least compared with the corresponding forced convection problem, is the approximation of the boundary conditions (9c), since the region covered by the finite difference mesh system must obviously be restricted to finite values of r. The simplest and most common approach, which has been widely utilized in studies of fluid mechanics alone (for example, Rimon, 1969; Son and Hanratty, 1969; Dennis and Chang, 1970; Masliyah and Epstein, 1970; Leal, 1973b), is simply to use the uniform stream conditions (9c) applied at a large but finite value of r (or equivalently, of ξ). Numerical experimentation showed this method to be computationally feasible in the present case also, provided $Gr \geqq 0$. Unfortunately, however, for $Gr < 0$ this simple approach was found to be entirely unsatisfactory. In this case, as the fluid passes above the plate, it is cooled and thus becomes stably stratified. As a result the fluid in the wake region downstream is also stably stratified and hence exhibits the phenomenon common to such flows of very strong upstream propagation of disturbances (see Long, 1953, 1955, 1972; Janowitz, 1968). For this reason, the solution close to the plate becomes much more sensitive to errors in the downstream boundary conditions than for the corresponding flow with $Gr > 0$. Thus, the uniform stream conditions are not adequate for numerical solution at least in the sense that the values of ξ_∞ required to ensure an accurate solution near the plate are too large to be economically feasible. After considerable trial and error, two alternative approaches were found to produce satisfactory results. The first involves the use of a far-field correction to the simple free stream condition, which is the first term of an infinite series expansion that converges asymptotically for $\xi >> 1$. Imai (1951) and Chang (1961) have discussed this far-field correction in some detail for the fluid mechanics problem alone ($Gr = 0$), and we have utilized the formalism of Chang to obtain a similar correction in the present case in which the buoyancy contribution plays an important role. The details of this calculation will be reported in a future communication. For the present purposes it is enough simply to quote the results

$$\left.\begin{aligned} &\theta \sim Ayx^{-3/2}\exp(-PrRey^2/4x) + o(r^{-1/2}); \quad x > 0 \\ &\theta = 0; \quad x < 0 \end{aligned}\right\} \tag{14}$$

$$\left.\begin{aligned} &\psi \sim y + \frac{m}{2\pi}\tan^{-1}\left(\frac{y}{x}\right) \\ &\quad + \sqrt{\frac{\pi}{PrRe}}\left\{\left[g(0) - \frac{K_1}{1-Pr}\right]\sqrt{Pr}\ \mathrm{erf}\left(\frac{\sqrt{Re}}{2}\frac{y}{\sqrt{x}}\right) + \frac{K_1}{1-Pr}\mathrm{erf}\left(\frac{\sqrt{PrRe}}{2}\frac{y}{\sqrt{x}}\right)\right\} + o(1); \quad x > 0 \\ &\psi \sim y + \frac{m}{2}\left[-1 + \frac{1}{\pi}\tan^{-1}\frac{y}{x}\right]; \quad x < 0 \end{aligned}\right\} \tag{15}$$

$$\left.\begin{aligned} &\omega \sim \frac{Re}{2}\frac{y}{x^{3/2}}\left\{\left[g(0) - \frac{K_1}{1-Pr}\right]\exp\left(-\frac{Re}{4}\frac{y^2}{x}\right) + \frac{PrK_1}{1-Pr}\exp\left(-\frac{PrRe}{4}\frac{y^2}{x}\right)\right\} + o(r^{-1/2}); \quad x > 0 \\ &\omega = 0; \quad x < 0 \end{aligned}\right\} \tag{16}$$

in which

$$A \equiv \frac{x_0^{1/2}}{2}\left(Nu - \int_{-x_0}^{-1/2} \left.\frac{\partial\theta}{\partial y}\right|_{y=0} dx - \int_{1/2}^{x_0} \left.\frac{\partial\theta}{\partial y}\right|_{y=0} dx \right)$$

$$K_1 \equiv A\frac{Gr}{Re^2}\cdot\frac{2}{PrRe}$$

$$g(0) \equiv -\frac{C_d}{2}\sqrt{\frac{Re}{\pi}} + K_1\left(\frac{1-\sqrt{Pr}}{1-Pr}\right)$$

$$m \equiv -\frac{2\sqrt{\pi}}{\sqrt{PrRe}}\left[\sqrt{Pr}\, g(0) + K_1\left(\frac{1-\sqrt{Pr}}{1-Pr}\right)\right]$$

In the latter expressions, Nu is the overall Nusselt number based on the total heat transfer at the upper surface of the plate,

$$Nu \equiv -\int_0^{\pi} \left.\frac{\partial\theta}{\partial\xi}\right|_{\xi=0} d\eta \qquad (17)$$

and C_d is the corresponding drag coefficient

$$C_d \equiv -\frac{1}{Re}\int_0^{\pi} \omega_0 \sin\eta\, d\eta \qquad (18)$$

Finally, in evaluating the expressions (14) to (16) at a particular point (x, y), the value x_0 is utilized to denote the x-intercept of the circular arc $r = (x^2 + y^2)^{1/2} =$ constant. It should be noted that the parameter A vanishes as $x_0 \to \infty$. In view of the definitions (17) and (18) it may be seen that the parameters A and $g(0)$ provide a direct coupling between the far-field solutions (14) to (16) and the numerical solution near the plate. The key idea in utilizing the far-field corrections at a large but finite value of r instead of the simple free stream conditions at the same position is to minimize the difference between the imposed values of ψ, ω, and θ, and the values which would exist at the same position if one had an exact solution. Using (14) to (18), the choice of ξ_∞ required for an accurate solution near the plate was reduced to an economically feasible value in all cases. The values used are listed in Table 1 ($x_\infty = \frac{1}{2}\cosh\xi_\infty$). We estimate these as the minimum value necessary to produce accurate solutions in the vicinity of the plate. In most cases, these values were actually confirmed by comparison with a similar solution obtained using the somewhat larger (or smaller) values listed in parentheses under x_∞ in Table 1. For $Gr = 0$, the values of x_∞ chosen correspond to those independently determined by Leal and Acrivos (1969) for a similar fluid mechanics problem. In addition, we note that the values listed in Table 1 are essentially equivalent to those utilized by Takami and Keller (1969) for flow past a circular cylinder with a similar wake correction when account is taken of the overall length of the cylinder plus the attached closed-streamline wake. It is noteworthy that the required distance decreases as Re increases, all else being fixed, while generally increasing as Gr is decreased to negative values or as Pr is decreased.

As an alternative to the far-field correction, the recently developed Milne's extrapolation procedure was also utilized to produce boundary values at ξ_∞ from the internal solution itself. Denoting the value of θ at $\xi = \xi_\infty - mh$ as θ_{N-m}, Milne's procedure for extrapolation outward in ξ along a line of constant η is defined by

$$\theta_N = \theta_{N-5} - 5\theta_{N-4} + 10\theta_{N-3} - 10\theta_{N-2} + 5\theta_{N-1} + 0(h^5) \qquad (19)$$

Similar expressions can be written for the streamfunction and vorticity. This formula, which was first derived by Lin and Apelt (1970), is based on the familiar Milne's predictor formula used to integrate ordinary differential equations (Lapidus and Seinfeld, 1971). The chief advantage of (19) compared with extrapolation schemes which have been previously proposed for estimating ψ, ω, and θ at the outermost boundary (compare Thoman and Szewczyk, 1969; Estoque, 1962; Yamada and Meroney, 1971), is that no explicit (and unjustified) assumption need be made of the functional dependence of these variables on ξ other than simple differentiability. The chief disadvantage of the extrapolation formulation compared with the scheme involving (14) to (18) is that the numerical algorithm is less stable, and distortions in the fields are produced if the initial fields are too inaccurate (Lin and Apelt 1970; Yamada and Meroney, 1971). On the other hand, the advantage of the extrapolation scheme is that the solution near the outer boundary is not directly coupled with that near the plate. In view of the unusually strong interaction already inherent in the stably stratified wake flow when the plate is cold, one may logically ask whether, in using (14) to (18), an incorrect value for C_d or Nu leading to an inaccurate boundary-value for $\xi = \xi_\infty$ at some intermediate point in the calculation might not lead to further inaccuracies in C_d or Nu and hence to some convergent but inaccurate solution in the vicinity of the plate. In order to ensure that this possibility did not actually occur, the calculations for the cold plate were first carried to near-convergence utilizing the stable far-field approximations, and then run to completion using both the far-field solutions and the extrapolation scheme independently. In general, the solutions so obtained were virtually identical. However, as Gr was made increasingly negative some small (2 to 3%) differences were noted in the vorticity distribution near the plate and, hence, by (18), in the drag coefficients as well. In these instances, the results reported here are based on the solution obtained using the extrapolation procedure since these appeared to introduce somewhat smaller disturbances in the flow near ξ_∞.

Finally, it should be mentioned that convergence was achieved via an oscillatory mode similar to that described previously by Leal and Acrivos (1969) and Leal (1973b). Thus, for example, C_d was observed to oscillate with a monotonically decreasing amplitude about a fixed mean and a characteristic period of 0(100) iterations. Such oscillatory convergence is very appealing as upper and lower bounds on the various dependent variables are available throughout the calculation. The solution was generally assumed to have converged when these bounds were within 0.05% of the average value for C_d and Nu. However, the detailed fields for ψ, θ, and ω were also examined carefully to ensure that the solutions were uniformly convergent throughout the (x, y) plane.

COMPARISON WITH PREVIOUS SOLUTIONS

A variety of detailed tests were performed to ensure the accuracy of the solutions reported here. Considering first of all the case of forced convection $Gr = 0$ in which the fluid mechanics is uncoupled from the heat transfer problem, we may compare our results for $Re = 10$, 40, and 100 directly with those obtained by Dennis and Dunwoody (1966) who studied the fluid mechanics problem alone.

The values of C_d shown in Figure 2 for these cases are virtually identical with those of Dennis and Dunwoody. Furthermore, the variation of the local skin friction coefficient $-\omega_0$, as a function of position along the plate agrees closely with that reported by these authors.

There are no prior results of which we are aware for forced convection heat transfer with $\theta = 0$ on $y = 0$, $|x| > \frac{1}{2}$. However, Dennis and Smith (1966) have considered the case in which $\partial\theta/\partial y = 0$ on $y = 0$, $|x| > \frac{1}{2}$. Hence, we also solved this problem in order to provide a test for the accuracy of our numerical algorithm. Again, the values of Nu, which are reported in Table 2, and the variation of the local heat transfer coefficient, $-2\ \partial\theta/\partial\xi|_{\xi=0}/\sin\eta$, with position along the plate surface, agree very well with the results of Dennis and Smith. The numerical results for the case in which $\theta = 0$ on $y = 0$ and $Gr = 0$ are also qualitatively similar to those of Dennis and Smith. However, as expected on physical grounds, the actual numerical values for the local heat transfer coefficient are somewhat larger, particularly near the ends of the plate.

A further test on the accuracy of our numerical scheme is provided by examining the Reynolds number dependence of δ_θ, the dimensionless vertical distance between the plate surface at $x = 0$ and the isotherm $\theta = 0.1$. δ_θ is a measure of the thickness of the thermal layer and is given in Table 3 for $Pr = 0.7$ and $Gr = 0$. It may be seen that δ_θ is roughly proportional to $Re^{-1/2}$, which is the theoretically predicted boundary-layer behavior (though, of course, quantitative agreement with boundary-layer theory is not obtained or expected for $Re \leq 100$).

Finally, as indicated previously, we have obtained a limited number of solutions for $Pr = 10$ and 0.1 in order to evaluate the effect of this parameter on the overall flow structure. In Figure 3, we have plotted the numerical results for $Gr = 0$ and $Re = 100$ together with the classical boundary-layer estimates for $Pr << 1$, $Pr = 1$, and $Pr >> 1$. These provide further evidence for the validity of the numerical scheme in the sense that the solutions for $Pr = 0.7$ and $Pr = 10$ appear to be consistent with the expected asymptotic trends. The result for $Pr = 0.1$ is also qualitatively correct but appears to somewhat overestimate the actual value. The most likely explanation for this behavior is that the outer boundary (ξ_∞) is not sufficiently far away from the plate. This is suggested by the fact that the solution still changed somewhat as x_∞ was increased from twice to three times its value at $Pr = 0.7$. Unfortunately, the excessive computation times involved for such large values of ξ_∞ (at this Reynolds number and Prandtl number) preclude any attempt to consider larger values of ξ_∞ directly. We shall return to discuss these results in more detail in the next section of this paper.

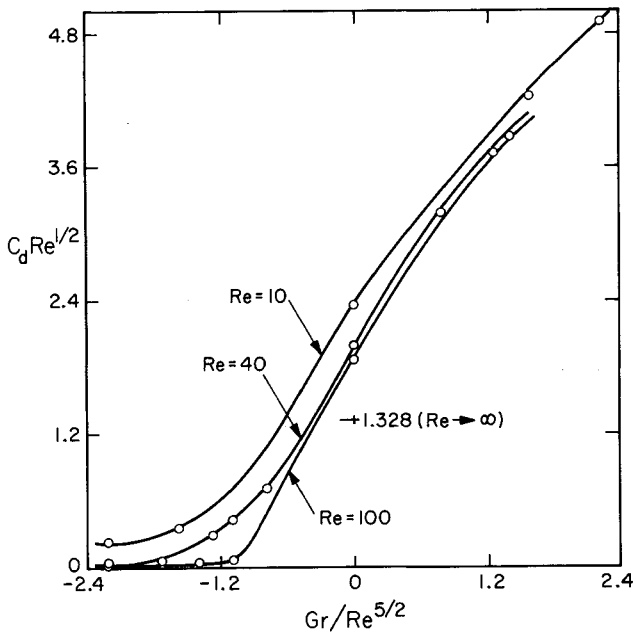

Fig. 2. $C_dRe^{1/2}$ as a function of the boundary-layer parameter, $Gr/Re^{5/2}$, for $Pr = 0.7$.

TABLE 2. Nu FOR $Gr = 0$, $Pr = 0.7$, AND $\partial\theta/\partial y = 0$ ON $y = 0$, $|x| > 1/2$

Investigators	$Re = 10$	$Re = 40$	$Re = 100$
Dennis and Smith	2.43	4.37	6.75
Present	2.43	4.32	6.74

TABLE 3. δ_θ FOR $Gr = 0$, $Pr = 0.7$

Re	10	40	100
δ_θ	0.86	0.41	0.26

TABLE 4. $C_dRe^{1/2}$ AND $NuRe^{-1/2}$ FOR $Pr = 10.0$ AND $Re = 40$

$Gr/Re^{5/2}$	−1.74	0	1.265
$C_dRe^{1/2}$	1.56	2.00	2.22
$NuRe^{-1/2}$	1.85	1.94	1.98

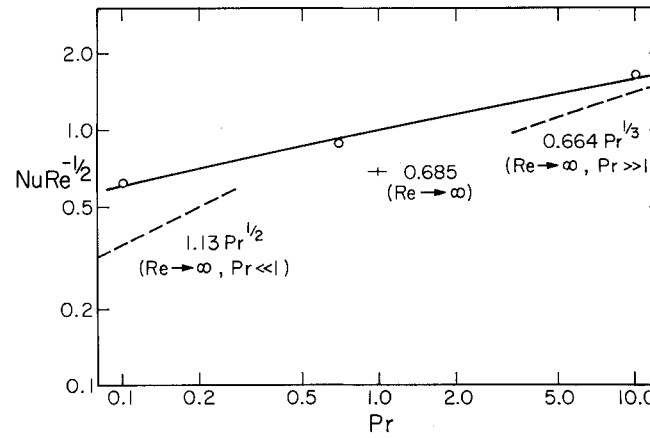

Fig. 3. $NuRe^{-1/2}$ as a function of Pr for $Gr = 0$: comparison of the numerical results for $Re = 100$ and the boundary-layer estimates for $Pr << 1$, $Pr = 1$, and $Pr >> 1$.

RESULTS AND DISCUSSION

We previously mentioned the expected boundary-layer flow structure for large Re, and $|Gr/Re^{5/2}|$* suitably small. In particular, we have noted that the cross-stream buoyancy force acts effectively to produce a streamwise pressure gradient at the upper plate surface which is favorable in the usual boundary-layer sense when the plate is hot and adverse when it is cold. Hence, the local boundary-layer flow is either accelerated or decelerated relative to the corresponding forced convection flow, with a concurrent increase or decrease in the local skin friction and heat transfer rates, depending upon whether the plate is hot or cold.

* Note that whereas the original Equation (1) depends on the parameters Re, Pr, and Gr/Re^2, the corresponding laminar boundary-layer equations for Pr = 0(1) contain only Pr and $Gr/Re^{5/2}$ as explicit parameters.

The main thrust of the present work has been to determine the effect of buoyancy on the flow structure and temperature distribution under circumstances in which $Gr/Re^{5/2}$ (and hence the natural convection contribution to the flow) is not necessarily small. In the first part of this section, we consider the effect of variable Re and Gr/Re^2 at a fixed value of $Pr = 0.7$. In the second, we briefly examine the change in flow structure as Pr is increased to 10 and decreased to 0.1 with $Re = 40$ and 100, and values of Gr/Re^2 equal to 8, 0, and -11. Finally, in the last part of this section we consider, in some detail, the structure of the recirculating eddy which results from flow separation at sufficiently negative values of Gr/Re^2.

Effects of Gr and Re on Flow Structure; Fixed $Pr = 0.7$

In order to achieve a relatively complete description of the dependence of the flow structure and temperature distribution on Re and Gr/Re^2 we have obtained steady state numerical solutions for $Re = 10$, 40, and 100 and a variety of positive and negative values of Gr/Re^2 as listed in Table 1. Typical streamline, vorticity and temperature plots are shown in Figures 4, 5, and 6, respectively, for $Re = 40$, $Pr = 0.7$ and $Gr/Re^2 = 8$, 0, -5 and -14. The flow is from left to right. Three features are worthy of special note. First, as expected from the boundary layer analyses (Sparrow and Minkowyz, 1962; Leal, 1973a), the gravitationally induced streamwise pressure gradient produces either an acceleration or deceleration of the flow near the plate with an accompanying narrowing or thickening of the boundary-layer region depending upon whether Gr is positive or negative (that is, the plate surface is hot or cold). When the surface temperature is sufficiently low (Gr sufficiently negative), the boundary flow actually separates and a recirculating eddy develops adjacent to the plate surface. Second, and perhaps the most interesting result from the numerical solutions, is the fact that this recirculating region can actually extend considerably upstream beyond the leading edge of the plate. Such a degree of upstream influence of the flat plate upon the basic flow structure seems to be an unex-

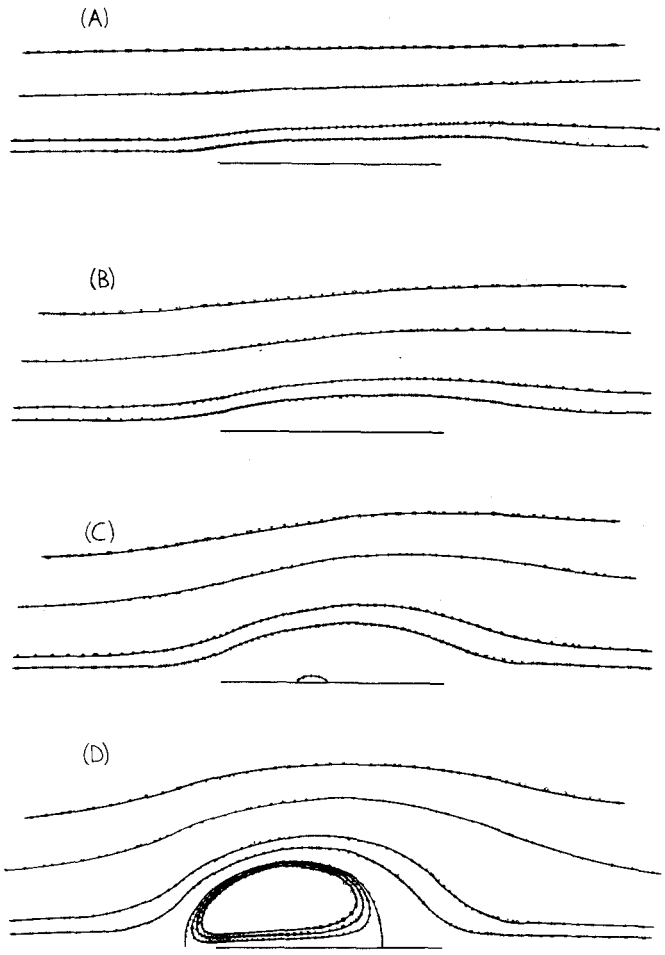

Fig. 4. Streamlines for $Re = 40$ and $Pr = 0.7$; $\psi = 0.5$, 0.3, 0.1, 0.05, 0, -0.005, -0.01, and -0.015 with 0.5 corresponding to the outermost streamline: (A) $Gr/Re^2 = 8$; (B) $Gr/Re^2 = 0$; (C) $Gr/Re^2 = -5$; (D) $Gr/Re^2 = -14$.

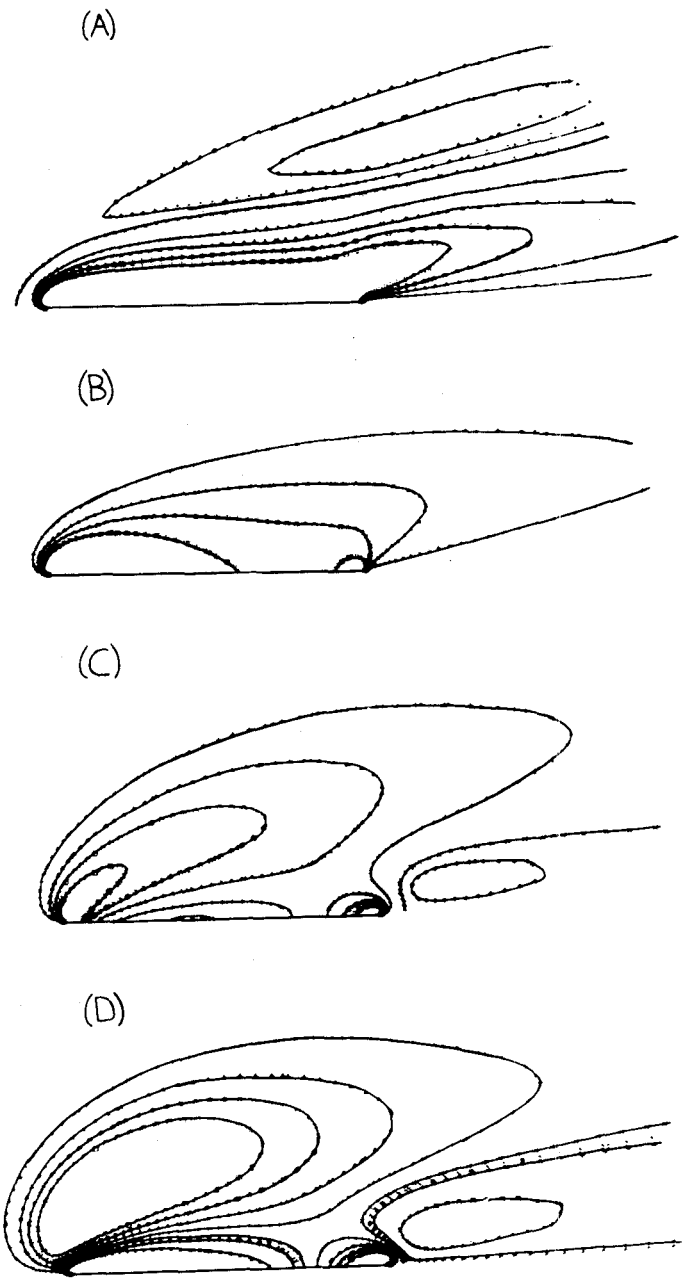

Fig. 5. Equivorticity lines for $Re = 40$ and $Pr = 0.7$: (A) $Gr/Re^2 = 8$; $\omega = -4$, -3, -2, -1, 0, 0.3, and 0.5 with -4 corresponding to the innermost curve; (B) $Gr/Re^2 = 0$; $\omega = -4$, -3, -2, and -1 with -1 corresponding to the outermost curve; (C) $Gr/Re^2 = -5$; $\omega = -4$, -3, -2, and -1 over the front and rear of the plate; $\omega = 0$ and 0.3 in the reverse flow region and downstream from the plate; (D) $Gr/Re^2 = -14$; $\omega = -4$, -3, -2, and -1 over the front and rear of the plate; $\omega = 0$, 0.5, and 2.0 in the reverse flow region and downstream from the plate.

pected and highly significant feature of the present problem, which we shall discuss in more detail at the end of this section. Thirdly, we note the existence, for $Gr \neq 0$, of closed equivorticity curves in the plots of Figure 5, indicating the presence of internal (nonboundary) sources for vorticity in these cases. The origin of these sources is the temperature induced density variations in the fluid, as can be easily seen from the vorticity transport equation for two-dimensional flow, namely,

$$\frac{\partial \omega}{\partial t} + u\frac{\partial \omega}{\partial x} + v\frac{\partial \omega}{\partial y} = \frac{1}{Re}\nabla^2\omega + \frac{Gr}{Re^2}\frac{\partial \theta}{\partial x}$$

The rate of vorticity production by variations in fluid density is given by $(Gr/Re^2)\dfrac{\partial \theta}{\partial x}$. In the upstream and downstream portions of the field, $\partial\theta/\partial x > 0$ and $\partial\theta/\partial x < 0$, respectively (see Figure 6). Hence, we expect that positive (negative) vorticity will be created on the upstream side for $Gr > 0$ ($Gr < 0$), and similarly negative (positive) vorticity on the downstream side for $Gr > 0$ ($Gr < 0$); our results exhibit these features. The vorticity distribution at steady state and $Gr \neq 0$ thus represents a balance between convection and diffusion of vorticity produced by the internal source at each point, as well as that produced at the plate boundary. A discussion of vorticity production in density stratified flow under more general circumstances is available in Yih (1965, 1969).

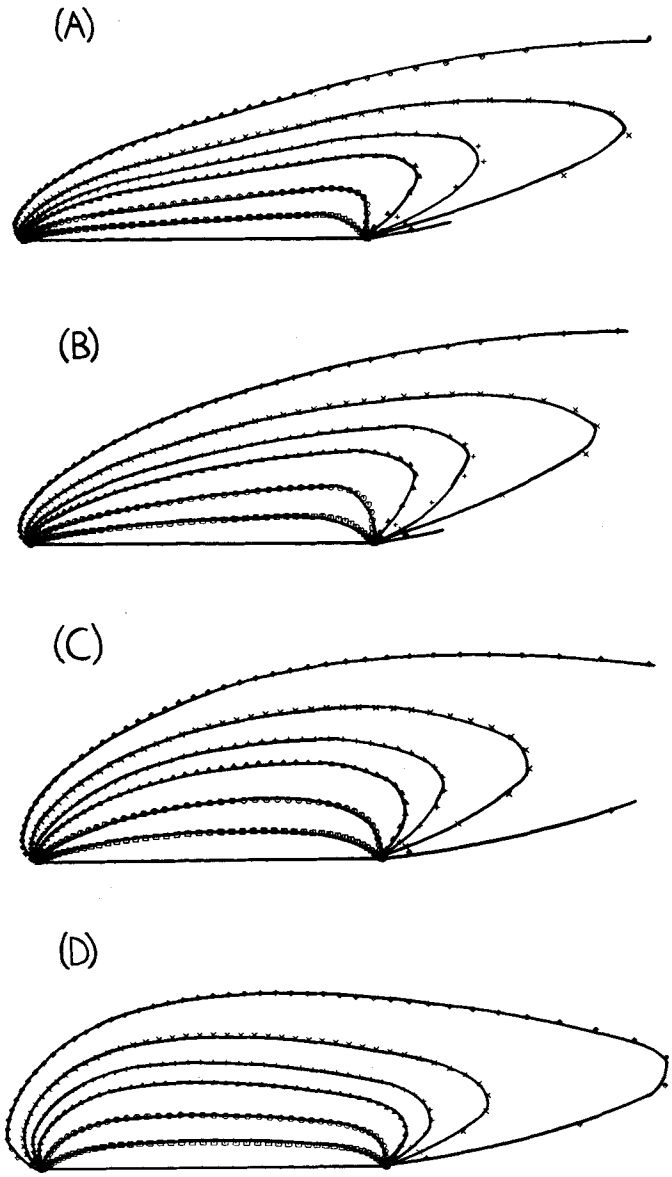

Fig. 6. Isotherms for $Re = 40$ and $Pr = 0.7$; $\theta = 0.8, 0.6, 0.4, 0.3, 0.2$, and 0.1 with 0.8 corresponding to the innermost isotherm: (A) $Gr/Re^2 = 8$; (B) $Gr/Re^2 = 0$; (C) $Gr/Re^2 = -5$; (D) $Gr/Re^2 = -14$.

The qualitative dependence of flow structure on Gr for $Re = 10$, 100, and $Pr = 0.7$ is similar to that described above for $Re = 40$. However, it is of interest to document more fully the dependence of flow structure on Re in order to provide an indication of the degree to which the small Gr boundary-layer behavior ($Pr = 0(1)$) of Sparrow and Minkowycz (1962) is preserved when Re is moderate and the natural convection effects are not intrinsically assumed to be small. Two overall parameters which have been frequently used to characterize the gross flow structure in problems of this sort are the drag coefficient C_d and Nusselt number Nu which we have defined in Equations (17) and (18). Figure 2 shows the dependence of $C_dRe^{1/2}$ on the boundary-layer parameter $Gr/Re^{5/2}$ for the various Reynolds numbers studied. For $|Gr/Re^{5/2}| << 1$ and fixed, and large Re, it is expected from boundary-layer theory that $C_dRe^{1/2}$ will be independent of Re. Surprisingly, even for Re as small as 40-100, $C_dRe^{1/2}$ appears to be qualitatively consistent with this behavior not only in the regime of small (positive) $Gr/Re^{5/2}$ but throughout the range studied up to +2.215. It should be noted, however, that $Re = 100$ is not sufficiently large to provide a quantitative comparison with boundary-layer behavior as evidenced by the fact that the value of $C_dRe^{1/2}$ calculated for $Gr = 0$, $Re = 100$ is still considerably above the theoretical boundary layer value of 1.328 (Dennis and Dunwoody, 1966). The divergence of the curves for negative Gr is viewed by us as a direct consequence of the existence of flow separation which corresponds to a total breakdown of the boundary-layer type flow structure which appears to be present for $Gr > 0$, even when $Gr/Re^{5/2}$ is not small. More interesting than the Reynolds number dependence is the very strong dependence of $C_dRe^{1/2}$ on Gr and particularly the very small although positive values of C_d which result for Gr negative and numerically large in absolute value. Although admittedly unusual from the point of view of classical fluid dynamics, the latter might be expected on physical grounds since the existence of a large recirculating eddy of the type pictured in Figure 4d implies that a large portion of the plate surface is subjected to reverse flow and, hence, negative skin friction. Figure 7 shows the calculated dependence of $NuRe^{-1/2}$ on $Gr/Re^{5/2}$ for $Re = 10$, 40, and 100. Clearly, the basic behavior is similar to that of the drag coefficient although the dependence on Gr is weaker and the dependence on Re somewhat stronger. The weak dependence on Gr is consistent with the boundary-layer predictions of Sparrow and Minkowycz (1962).

Effect of Pr on Flow Structure; Fixed Re and $Gr/Re^{5/2}$

Recently, Leal (1973a) considered the asymptotic boundary-layer structure for the present problem in the limits as $Pr \to \infty$ and $Pr \to 0$, respectively for $|Gr/Re^{5/2}|$ suitably restricted. The key qualitative result from this work was the suppression or enhancement of the buoyancy effect depending upon whether $Pr >> 1$ or $Pr << 1$, respectively, which arises from the fact that the thermal boundary layer is either very thin or very thick relative to the momentum boundary layer in these limits. When $Pr >> 1$ and the thermal layer is thin, the buoyancy driving force is confined essentially to the viscous layer near

the wall, and its effect on the dynamics is thereby diminished compared with the case $Pr = 1$. On the other hand, when $Pr << 1$, the thermal driving force is primarily effective in the nonviscous portion of the flow outside the momentum boundary-layer and its effect is thereby enhanced.

It is of interest to compare the qualitative dependence of the overall parameters $NuRe^{-1/2}$ and $C_dRe^{1/2}$ on Pr with the theoretical predictions from the boundary layer analysis of Leal (1973a). In Figure 3, we have plotted the numerical results for $Re = 100$ and $Gr = 0$ as discussed in the previous section. The finite value of Re is apparently reflected in the uniform upward displacement of the numerical results compared with the theoretical ones which are evident in the plot. In order to ascertain the practical effects of Pr on the flow dynamics for $|Gr/Re^{5/2}| = 0(1)$, numerical solutions were obtained at fixed $Re = 40$ and $Gr/Re^{5/2} = 1.265$, 0, and -1.74; Table 4 gives the results for $C_dRe^{1/2}$ and $NuRe^{-1/2}$ with $Pr = 10.0$. A dramatic example of the enhancement of the influence of buoyancy on the flow structure for decreasing Pr is that, for $Gr/Re^{5/2} = -1.74$, *no* separation occurs for $Pr = 10.0$ whereas a reverse flow region develops for $Pr = 0.7$ as will be evident from the next part of this section. For large and increasing Pr, Leal predicts that the corrections due to the buoyancy effect to the forced convection values of $C_dRe^{1/2}$ and $NuRe^{-1/2}$ should behave like $Pr^{-2/3}$ and $Pr^{-1/3}$, respectively. It is somewhat surprising in view of the restrictions on Gr which are implicit in the boundary-layer analysis that our results for $Gr/Re^{5/2} = 1.265$ exhibit qualitatively the same behavior (although the theory only requires that $Pr >> 1$ and $Gr/Re^{5/2} << Pr^{2/3}$). No attempt was made to obtain results at $Pr = 0.1$, in addition to the case $Re = 100$ and $Gr = 0$, in view of the large values of x_∞ required; however, it is expected that the results would be qualitatively similar for $Gr \geq 0$ to those predicted by the boundary-layer analysis of Leal.

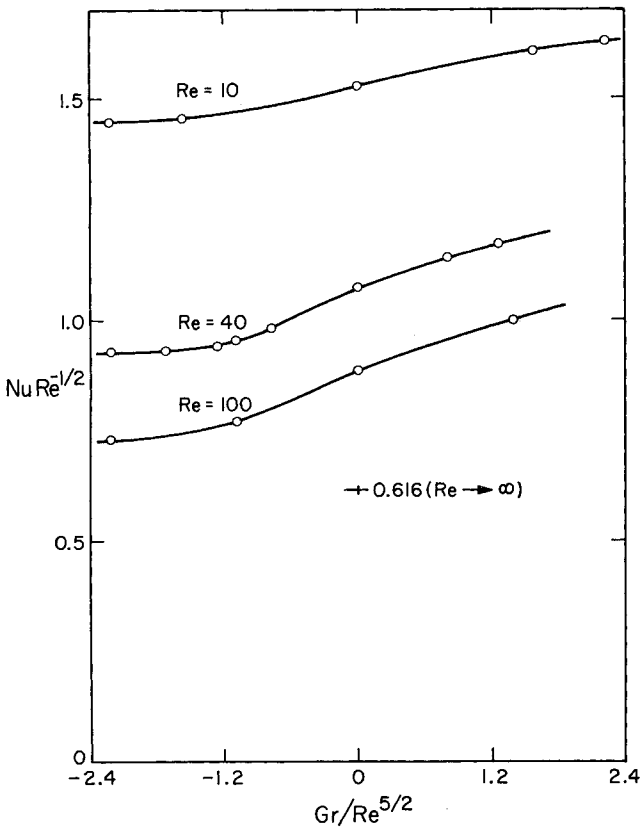

Fig. 7. $NuRe^{-1/2}$ as a function of the boundary-layer parameter, $Gr/Re^{5/2}$, for $Pr = 0.7$.

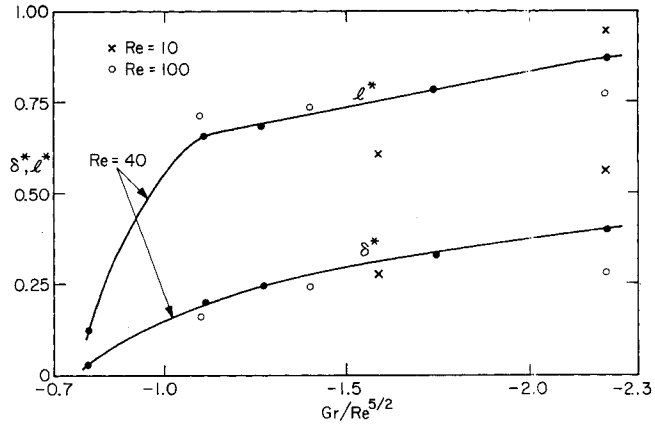

Fig. 8. δ^* and l^*, as a function of the boundary-layer parameter, $Gr/Re^{5/2}$, for $Pr = 0.7$.

Structure of the Recirculating Eddy; Fixed $Pr = 0.7$

We have previously noted that when the plate is cold and Gr is sufficiently large, the adverse pressure gradient which is induced causes the boundary flow to separate with the resultant formation of a recirculating eddy whose nominal dimensions may sometimes approach that of the plate. In the remainder of this section, we return to a more detailed consideration of the structure of this region for $Gr < 0$ and $Pr = 0.7$. In particular, we consider three geometric features of the recirculating eddy: the dimensionless overall length between its leading and trailing edges measured at $y = 0$ (l^*), the dimensionless maximum vertical height δ^*, and the dimensionless position of its leading edge x^*, again measured at $y = 0$. Since the inception of the separation process for large Re is governed by the boundary-layer equations, it should be expected that all of these physical features would have a common origin, independent of Reynolds number, when plotted against the sole boundary layer parameter $Gr/Re^{5/2}$, provided only that Re is sufficiently large.

In Figure 8, we have plotted δ^* as a function of $Gr/Re^{5/2}$ for $Re = 10$, 40, and 100. As expected, the numerical data do appear to collapse onto a universal curve for small values of $|Gr/Re^{5/2}|$, with a common origin of approximately -0.8. The continued correlation at higher $|Gr/Re^{5/2}|$ is possibly fortuitous since the boundary-layer theory is not directly applicable in this domain. The main additional feature of interest in Figure 8 is the monotonic increase in the vertical extent δ^* as the plate is increasingly cooled to lower temperatures. We have also observed very similar behavior for the overall length of the recirculating region l^* as shown in Figure 8. Finally, we turn to the streamwise position of the upstream edge of the recirculating eddy x^*, which is plotted as a function of $Gr/Re^{5/2}$ in Figure 9. Clearly, as we have noted previously, the recirculating region does extend upstream beyond the leading edge of the plate for a sufficiently cooled plate. However, the most significant feature of this plot is the fact that, at least through $Gr/Re^{5/2} = -2.3$, x^* is increasing monotonically with increasing values of $|Gr/Re^{5/2}|$. Whether this trend will continue as $|Gr/Re^{5/2}|$ increases is, of course, a question of some importance which the present work cannot answer.

The phenomena of buoyancy induced upstream influence is, of course, widely known to occur in circumstances where the entire fluid is stably stratified. A reasonably comprehensive discussion is presented by Yih (1965, 1969), following the initial, extensive work of Long (1953,

1955). However, so far as we are aware, the present investigation is the first to report such an effect which is completely due to locally produced density gradients. In the absence of this effect, one would expect the boundary separation to occur somewhere on the plate surface, certainly downstream of its leading edge. A logical question, therefore, is whether a mechanism is available which could possibly account for the leading edge of the recirculating eddy flow moving upstream in such a dramatic fashion. In order to investigate this point in detail, we numerically studied the time-dependent development of a reverse flow region for $Re = 10$ and $Pr = 0.7$ by starting with the forced convection solution ($Gr/Re^2 \equiv 0$) and changing instantaneously at $t = 0$ from this condition to $Gr/Re^2 = -7$. Several streamline and temperature plots for subsequent points in time are shown in Figures 10 and 11. These appear to suggest the following explanation for the locally-induced upstream influence effect. The fluid directly above the plate is stably stratified as a result of being cooled in passing over its surface. Initially the streamwise variations in the density profile produce only an adverse pressure distribution and the flow separates in the usual manner. For $Re = 10$, $Pr = 0.7$, and $Gr/Re^2 = -7$, the initial separation point is approximately $x_s = -0.25$. This separation leads to a recirculating eddy of finite cross section which the boundary flow must pass over. However, the flow upstream of x_s is stably stratified and the recirculating eddy thus tends to block the flow. This blockage (which is strictly a locally induced phenomenon) causes the pressure distribution to be modified upstream in such a way that the separation process is enhanced and

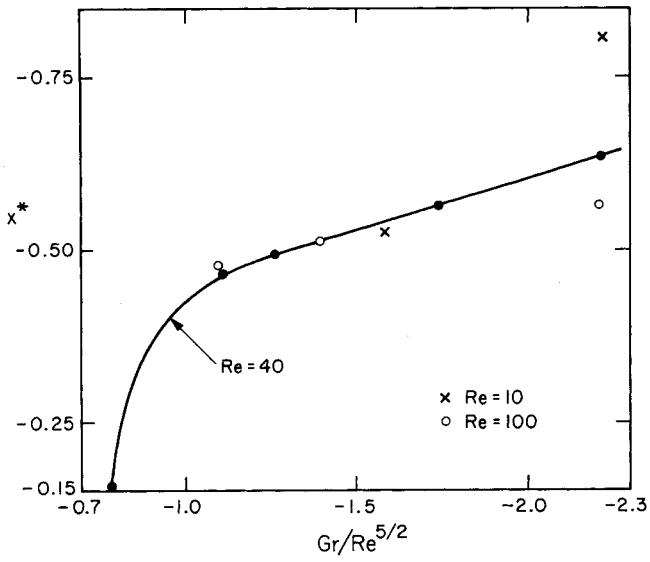

Fig. 9. x^* as a function of the boundary-layer parameter, $Gr/Re^{5/2}$, for $Pr = 0.7$.

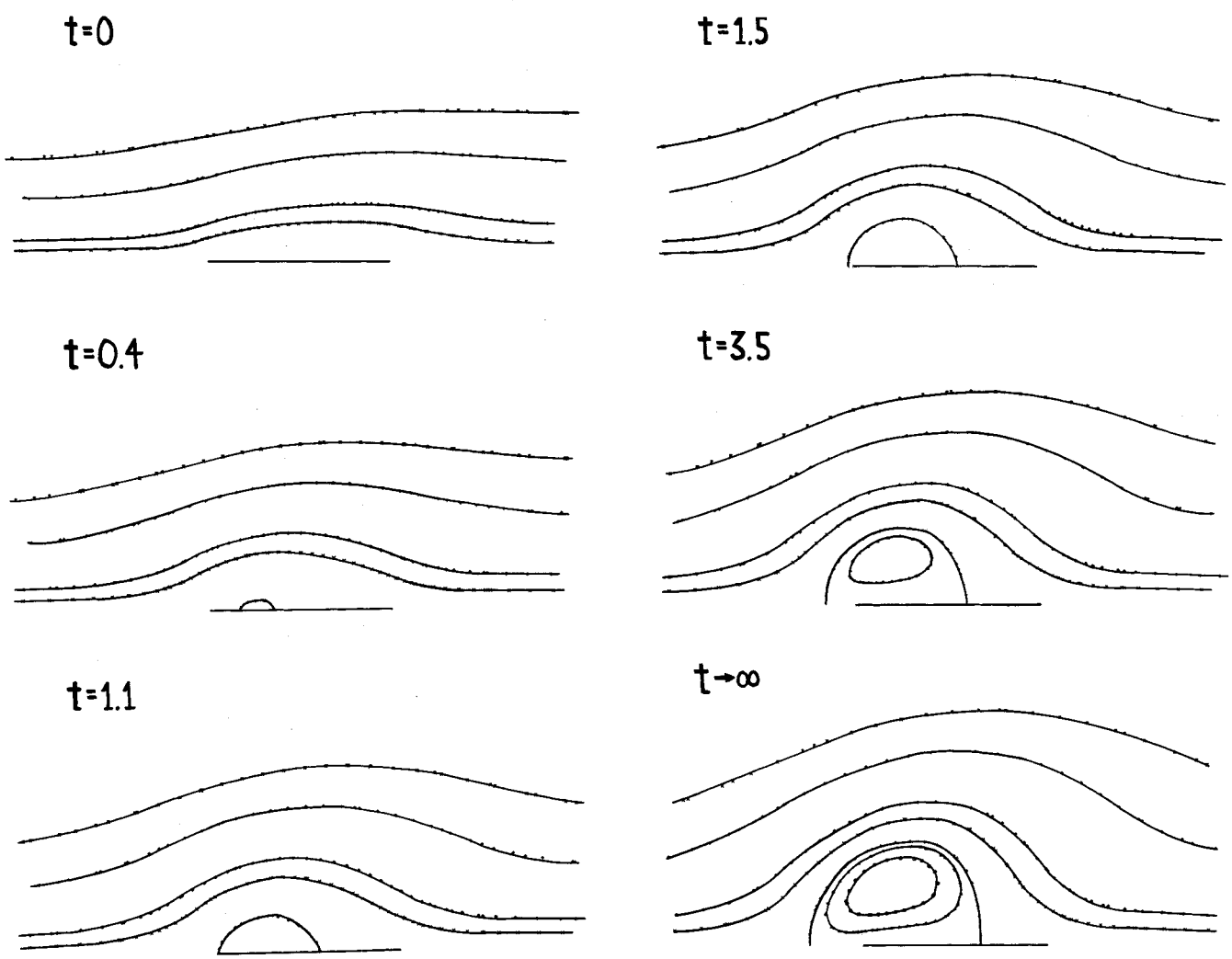

Fig. 10. Streamlines for $Re = 10$, $Pr = 0.7$, and $Gr/Re^2 = -7$; $\psi = 0.5, 0.3, 0.1, 0.05, 0, -0.01, -0.025$ with 0.5 corresponding to the outermost streamline.

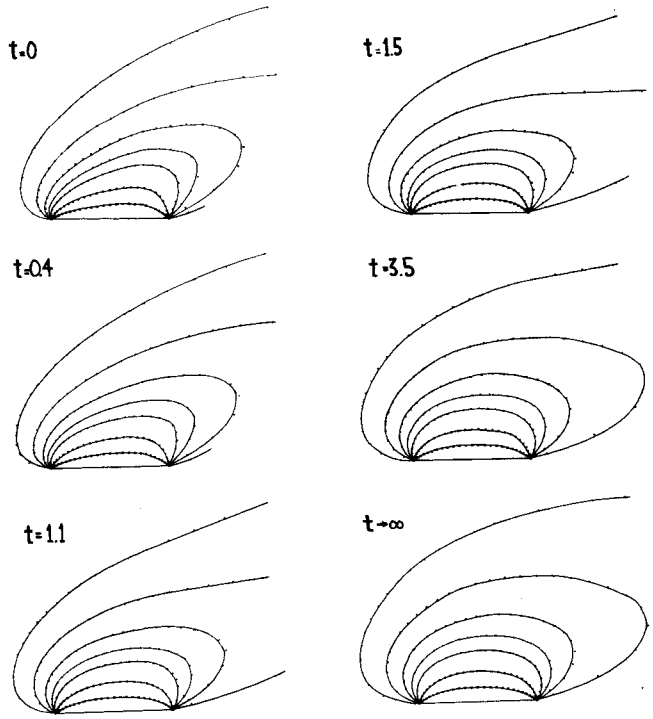

Fig. 11. Isotherms for $Re = 10$, $Pr = 0.7$, and $Gr/Re^2 = -7$; $\theta = 0.8, 0.6, 0.4, 0.3, 0.2, 0.1$, and 0.03 with 0.8 corresponding to the innermost isotherm

occurs more quickly. Ultimately, the leading edge of the eddy moves beyond the leading edge of the plate. At this point, the stratified fluid upstream can only be a result of local cooling of the fluid outside the eddy by the fluid inside. For a given fixed value of Gr, the upstream edge thus attains a finite equilibrium position. It is indeed significant from this point of view that the temperature field precedes the recirculating eddy in moving upstream; it is the region of stably stratified fluid that is produced which apparently allows the reverse flow region to propagate beyond the leading edge of the plate.

In conclusion, it will be of considerable interest to extend the present results to a locally induced flow stratification of the type reported here, coupled with an ambient free stream stratification. In this regard, it is of interest to note that Estoque (1962), in a large-scale numerical analysis of turbulent, stratified, boundary layer flow, predicted the presence of a recirculating region extending over land for an imposed prevailing breeze from warm land to a cool body of water.

ACKNOWLEDGMENT

This work was supported in part by National Science Foundation Grant GK-35476.

LITERATURE CITED

Acrivos, A., "On the Combined Effect of Forced and Free Convection Heat Transfer in Laminar Boundary Layer Flows," *Chem. Eng. Sci.*, **21**, 343 (1966).

Arakawa, A., "Computational Design for Long-Term Numerical Integration of the Equations of Fluid Motion: Two-Dimensional Incompressible Flow, Part I," *J. Comp. Phys.*, **1**, 119 (1966).

Boussinesq, J., *Theorie Analytique de la Chaleur*, Vol. 2, Gathier-Villars, Paris (1903).

Chang, I.-D., "Navier-Stokes Solutions at Large Distances from a Finite Body," *J. Math. Mech.*, **10**, 811 (1961).

Dennis, S. C. R., and G.-Z. Chang, "Numerical Solutions for Steady Flow past a Circular Cylinder at Reynolds Numbers up to 100," *J. Fluid Mech.*, **42**, 471 (1970).

Dennis, S. C. R., and J. Dunwoody, "The Steady Flow of a Viscous Fluid past a Flat Plate," *ibid.*, **24**, 577 (1966).

Dennis, S. C. R., and N. Smith, "Forced Convection from a Heated Flat Plate," *ibid.*, 509.

Estoque, M. A., "The Sea Breeze as a Function of the Prevailing Synoptic Situation," *J. Atm. Sci.*, **19**, 244 (1962).

Imai, I., "On the Asymptotic Behavior of Viscous Fluid Flow at a Great Distance from a Cylindrical Body, with Special Reference to Filon's Paradox," *Proc. Roy. Soc. London*, **A208**, 487 (1951).

Janowitz, G. S., "On Wakes in Stratified Fluids," *J. Fluid Mech.*, **33**, 417 (1968).

Janssen, E., "Flow past a Flat Plate at Low Reynolds Numbers," *ibid.*, **3**, 329 (1957).

Lapidus, L., and J. H. Seinfeld, *Numerical Solution of Ordinary Differential Equations*, Academic Press, New York (1971).

Leal, L. G., "Combined Forced and Free Convection Heat Transfer from a Horizontal Flat Plate," Z.A.M.P., in press (1973a).

———., "Steady Separated Flow in a Linearly Decelerated Free Stream," *J. Fluid Mech.*, in press (1973b).

———., and A. Acrivos, "Structure of Steady Closed Streamline Flows within a Boundary Layer," *Phys. Fluids Supplement II*, **12**, II-105 (1969).

Lin, J.-T., and C. J. Apelt, "Stratified Flow over an Obstacle; A Numerical Experiment," Project THEMIS, Tech. Rept. No. 7, CER69-70JTL-CJA25, Fluid Dynamics Diffusion Lab., Colorado St. Univ., Fort Collins (1970).

Long, R. R., "Some Aspects of the Flow of Stratified Fluids. I A Theoretical Investigation," *Tellus*, **5**, 42 (1953).

———., "Some Aspects of the Flow of Stratified Fluids. III Continuous Density Gradients," *ibid.*, **7**, 341 (1955).

———., "Finite Amplitude Disturbances in the Flow of Inviscid Rotating and Stratified Fluids over Obstacles," in *Ann. Review of Fluid Mechanics*, Vol. 4, p. 69, Annual Reviews, Palo Alto, Cal. (1972).

Masliyah, J. H., and N. Epstein, "Numerical Study of Steady Flow Past Spheroids," *J. Fluid Mech.*, **44**, 493 (1970).

Merkin, J. H., "The Effect of Buoyancy Forces on the Boundary-Layer Flow over a Semi-Infinite Vertical Flat Plate in a Uniform Free Stream," *ibid.*, **35**, 439 (1969).

Rimon, Y., "Numerical Solution of the Incompressible Time-Dependent Viscous Flow past a Thin Oblate Spheroid," *Phys. Fluids Supplement II*, **12**, II-65 (1969).

Son, J. S., and T. J. Hanratty, "Numerical Solution for the Flow around a Cylinder at Reynolds Numbers of 40, 200, and 500," *J. Fluid Mech.*, **35**, 369 (1969).

Sparrow, E. M., and W. J. Minkowycz, "Buoyancy Effects on Horizontal Boundary-Layer Flow and Heat Transfer," *Intern. J. Heat Mass Transfer*, **5**, 505 (1962).

Spiegel, E. A., and G. Veronis, "On the Boussinesq Approximation for a Compressible Fluid," *Astrophys. J.*, **131**, 442 (1960).

Takami, H., and H. B. Keller, "Steady Two-Dimensional Viscous Flow of an Incompressible Fluid Past a Circular Cylinder," *Phys. Fluids Supplement II*, **12**, II-51 (1969).

Thom, A., and C. J. Apelt, "Note on the Convergence of Numerical Solutions of the Navier-Stokes Equations," Aeronautical Res. Council Rep. Mem. (GB), No. 3061 (1956).

Thoman, D. C., and A. A. Szewczyk, "Time-Dependent Viscous Flow Over a Circular Cylinder," *Phys. Fluids Supplement II*, **12**, II-76 (1969).

Yamada, T., and R. N. Meroney, "Numerical and Wind Tunnel Simulation of Response of Stratified Shear Layers to Nonhomogeneous Surface Features," Project THEMIS, Tech. Rept. No. 9, CER-70-71TY-RNM62, Fluid Dynamics Diffusion Lab., Colorado St. Univ., Fort Collins (1971).

Yih, C.-S., *Dynamics of Nonhomogeneous Fluids*, MacMillan Co., New York (1965).

———., "Stratified Flows," in *Annual Review of Fluid Mechanics*, p. 79, Vol. 1, Annual Reviews, Palo Alto, Cal. (1969).

Manuscript received March 2, 1973; revision received May 3 and accepted May 4, 1973.